Superdense state of the monolayer hydrogen on adsorbent under liquefied temperature

Hiroyuki Gi
Yuki Kashiwara
Hiroshima University
Yuki Itoh
Hiroshima University
Khushbu Sharma
Hiroshima University
Norio Ogita
Hiroshima University
Hiroki Miyaoka
Hiroshima University
Tomofumi Ogawa
Air Liquide
Marolop Simanullang
Air Liquide
Laurent Prost
Air Liquide
Takayuki Ichikawa (tichi@hiroshima-u.ac.jp)
Hiroshima University

Article

Keywords:

Posted Date: May 5th, 2022

DOI: https://doi.org/10.21203/rs.3.rs-1564476/v1

Superdense state of the monolayer hydrogen on adsorbent under liquefied temperature

[1]Hiroyuki Gi, [1]Yuki Kashiwara, [1]Yuki Itoh, [1]Khushbu Sharma, [1]Norio Ogita, [1,2] Hiroki Miyaoka,

[3]Tomofumi Ogawa, [3]Marolop Simanullang, [3]Laurent Prost, [1,2,4]Takayuki Ichikawa*

[1]Graduate School of Advanced Science and Engineering, Hiroshima University, 1-4-1 Kagamiyama, Higashi-Hiroshima, 739-8527, Japan

[2]Natural Science Center for Basic Research and Development, Hiroshima University, 1-3-1 Kagamiyama, Higashi-Hiroshima 739-8530, Japan

[3]Air Liquide, Research & Development, Innovation Campus Tokyo, 2-2 Hikarinooka, Yokosuka, Kanagawa 239-0847, Japan

[4]A-ESG Science and Technology Research Center, Hiroshima University, 1-4-1, Kagamiyama, Higashi-Hiroshima 739-8527, Japan

*Corresponding author: Takayuki Ichikawa, tichi@hiroshima-u.ac.jp

Abstract

A systematic examination of the cryogenic H_2 adsorption properties below critical point of H_2 (T_c = 33 K) on a various kind of adsorbents was carried out, then the density of adsorbed H_2 on each adsorbent and its temperature dependence were experimentally compared with the liquid H_2. Usually, H_2 adsorption on porous materials was investigated at liquid nitrogen temperature (77 K) to realize its practical application for H_2 storage and most of reports have focused on the development of new porous materials. On the other hand, this work was focused for the first time on the cryogenic H_2 adsorption properties of metal organic frame works, superactivated carbon, and graphene nanoplatelets. We found superdense H_2 adsorption as the monolayer state, having much higher density than liquid H_2, which is contrary to the general understanding that the upper limit of adsorbed H_2 density is believed to the density of liquid H_2.

Introduction

Due to the world consensus toward carbon-neutrality by 2050, renewable energy such as wind, solar, and hydro power needs to be a mainstream power source. However, renewable energy supply is not good match to energy demand because of the lack of adjustment ability of the renewable energy. Some suitable energy storage devices, such as rechargeable batteries, pumped hydropower, heat storage, compressed air energy storage, and flywheel, are necessary. Hydrogen (H_2) is the most important candidate to realize not only energy storage but also energy transportation. Therefore, it has been widely recognized that a hydrogen based economy is necessary to realize a carbon-free society due to the H_2 ability of regenerative properties with zero emissions and high gravimetric energy density. However, the technology development of H_2 storage and transportation is major challenge for realization of hydrogen-based economy caused by its low volumetric energy density. In order to increase the volumetric and gravimetric energy density of H_2, following techniques have been considered: compressed H_2, liquid H_2, H_2 ab/adsorption in materials[1,2]. The physical properties of H_2 adsorption in porous materials have been investigated to realize its practical application. These adsorption properties are mainly controlled by the van der Waals interaction between H_2 molecule and the surface of materials[3–5]. Recent studies are focused on the development of porous materials having high surface area, appropriate pore size, and pore volume such as porous carbon materials[4,6–12], zeolites, and[13–17], metal organic flame works (MOFs)[11,18–23]. It's well known that the maximum H_2 uptake

strongly depends on the specific surface area of materials[6,11,14,19], and the density of adsorbed H_2 is believed to that of liquid H_2[6,9,11,24] as the upper limit. This indicates that the volumetric H_2 capacity using porous materials would never be superior to that of liquid H_2, no matter how high a specific surface area of the material is developed. Hence, H_2 adsorption tests under H_2 liquefaction conditions have rarely been performed and the detailed properties of cryogenic H_2 adsorption are not understood yet.

This work provides for the first time a systematic examination of the cryogenic H_2 adsorption properties below critical point of H_2 (T_c = 33 K) on a various kind of adsorbents, which are metal organic frame works (MOF-177), superactivated carbon (MSC-30) and graphene nanoplatelets (GNPs) as well as an explanation of the adsorption mechanism. The density of adsorbed H_2 on each adsorbent and its temperature dependence were experimentally examined and compared with the liquid H_2.

Results

Textural properties of adsorbents.

Textural properties of MOF-177, MSC-30 and GNPs were investigated by the nitrogen (N_2) adsorption-desorption isotherms (shown in Supplementary Fig.1) and were summarized in Table 1. The isotherms of MOF-177 and MSC-30 can be classified as Type I that are typical feature for adsorption on microporous adsorbents according to IUPAC classification scheme[25]. MOF-177 specially shows the steep uptake at low pressure (relative pressure of $P/P_0 \approx 0.01$) compared with MSC-30, indicating MOF-177 mostly has narrow micropores and MSC-30 has multilayer N_2 adsorption in wider micropores. For GNPs, the N_2 isotherm is classified as Type II that are typical for nonporous or macroporous adsorbents[25]. The specific surface area for each adsorbent having different pore structure was evaluated by applying the Brunauer–Emmett–Teller (BET) theory to the N_2 isotherms, resulting in 3950 m^2/g (MOF-177), 2860 m^2/g (MSC-30) and 810 m^2/g (GNPs). Total pore volume was evaluated 1.64 cm^3/g (MOF-177), 1.44 cm^3/g (MSC-30) and 1.27 cm^3/g (GNPs), following the trend of the gravimetric surface area. On the contrary to the trend of gravimetric surface area, volumetric surface area of MSC-30 was evaluated to higher value (7436 m^2/cm^3) than that of MOF-177 (6320 m^2/cm^3), because MSC-30 has higher real density as shown in Table 1.

Hydrogen adsorption at 20.4 K.

The cryogenic H_2 adsorption properties were investigated by comparing the introduced H_2 (i-H_2) amount into the cryogenic cell of 12.3 cm^3 with 2.22 g of MOF-177, 1.50 g of MSC-30, and 2.00 g of GNPs at 20.4 K, and the isothermal properties of H_2 introduction are shown in Fig.1. The isothermal curve of the blank result shows the characteristics of the pure H_2, which shows subtle increase in i-H_2 amount as gaseous H_2 below 0.1 MPa, and then i-H_2 amount simply increases without pressure change as the phase transformation from gas to liquid at 0.1 MPa. The volume occupied by liquid state H_2 in the blank measurement was evaluated to be 9.3 cm^3 based on the density of liquid and gaseous H_2 referred from the National Institute of Standards and Technology (NIST) website[26], where the liquefied H_2 was illustrated as blue color in Fig.1b. Because the top of cryogenic cell has slight temperature gradient, i-H_2 amount gradually increased with pressure increasing above 0.1 MPa. This phenomenon can be understood by the expansion of liquefied H_2 region, which was caused by satisfying the liquefaction conditions above H_2 boiling point (0.1 MPa and 20.4 K).

In the case of the isotherms with adsorbents of MOF-177, MSC-30 and GNPs, i-H_2 amount drastically increased by H_2 adsorption on adsorbents below 0.1 MPa as a main contribution. The inset graph in Fig. 1a shows the H_2 adsorption isotherms of the gravimetric H_2 uptake (wt.%), where the contributions of gaseous H_2 amount introduced into the dead volume were subtracted. The H_2 isotherms for all adsorbents are reversible and similar type to the N_2 isotherms, indicating there is no

significant difference in the apparent physical adsorption phenomenon for N_2 and H_2. The value of gravimetric H_2 uptake at 0.1 MPa for each adsorbent is listed in in Table.1 as well and it can be observed that the adsorbents with higher gravimetric surface area have the higher H_2 uptake following the trend in the previous research [6,11,14,19]. It is noteworthy that MOF-177 shows the highest gravimetric H_2 uptake of 14.8 wt.% at 0.1 MPa, which is much higher than 1.36 wt.% (at 0.1 MPa) and 11 wt.% (at 10 MPa) uptakes examined at 77 K by Saha et al.[27] .

At 0.1 MPa in Fig.1, liquefaction of H_2 starts, then the dead volume in the cell with a homogeneous temperature region at 20.4 K is filled with liquefied H_2 as shown in the image of Fig. 1b. Here, the i-H_2 amount with MSC-30 is almost equivalent to the i-H_2 amount of blank even though the H_2 molecules cannot occupy the volume with carbon atoms of MSC-30. In other words, the total volume of the blank cell, in which the H_2 molecule can exist, should be larger than that of the cell with MSC-30. According to this result, it can be expected that the density of adsorbed H_2 ($\rho_{ads.H_2}$) on MSC-30 is much higher than that of liquid H_2 ($\rho_{liq.H_2}$). It is interesting because it's contrary to the general understanding that the density of adsorbed H_2 is believed to that of liquid H_2[6,9,11,24] as the upper limit. Therefore, we suggest this anomalous H_2 adsorption at 20.4 K, and call it as "superdense H_2".

In order to quantitatively discuss the superdense state of H_2, we evaluated $\rho_{ads.H_2}$ on each adsorbent at 20.4 K, 0.1 MPa (see the "Evaluation of adsorbed H_2 density" in the supplementary information) and summarized in Table 1. Interestingly, $\rho_{ads.H_2}$ on all of adsorbents show higher

density than the liquid H_2 density ($\rho_{liq.H_2}$:35.2 mmol/cm^3) at the boiling point (20.4 K, 0.1 MPa), which are 34%, 23%, and 14% higher for MOF-177, MSC-30, and GNPs, respectively. In particular, $\rho_{ads.H_2}$ on MOF-177 and MSC-30 is comparable to and exceeds the solid H_2 density ($\rho_{sol.H_2}$: 43 mmol/cm^3), which is reported as a hexagonal close-packed (hcp) structures below 14 K[28–31].

Temperature dependence of H_2 adsorption below critical point.

We investigated the temperature dependence of isothermal properties of the H_2 introduction into the cell with MOF-177, MSC-30 and GNPs at 23.3, 26.5, 30.6 K in the same way as the experiment corresponding to Fig.1, and the results are shown in Fig. 2. All isotherms show similar adsorption and liquefaction steps at each temperature, where H_2 liquefied at 0.10 MPa (20.4 K), 0.22 MPa (23.3 K), 0.43 MPa (26.5 K), and 0.88 MPa (30.6 K). The i-H_2 amount above each phase transition pressure of blank tends to decrease with increasing temperature due to the physical properties of the liquid H_2 density, which are 35.2 mmol/cm^3 (20.4 K, 0.10 MPa), 33.3 mmol/cm^3 (23.3 K, 0.22 MPa), 30.9 mmol/cm^3 (26.5 K, 0.42 MPa), and 26.2 mmol/cm^3 (30.6 K, 0.87 MPa). The i-H_2 amount above each phase transition pressure with adsorbents also decrease with increasing temperature, however it is noteworthy that the i-H_2 amount with MOF-177 and MSC-30 gradually exceeds the value of blank with increasing temperature. These phenomena suggest that the temperature dependence of $\rho_{ads.H_2}$ is different from that of $\rho_{liq.H_2}$. In other words, the density of superdense H_2 state is less affected by temperature than the density of liquid H_2.

We quantitatively evaluated $\rho_{ads.H_2}$ at each temperature and on each adsorbent in the same way at 20.4 K described above (see the "Evaluation of adsorbed H_2 density" in the supplementary information), and the results are shown in Fig. 3 (see also Supplementary table.1) together with $\rho_{liq.H_2}$ at each phase transition point. It can be seen that $\rho_{ads.H_2}$ on any adsorbent shows the higher density than $\rho_{liq.H_2}$ at any temperature, and MOF-177 shows the highest $\rho_{ads.H_2}$, followed in order by MSC-30 and GNPs. Comparing the temperature change of $\rho_{ads.H_2}$, MOF-177 and MSC-30 don't significantly decrease with increasing temperature compared with the decreasing of $\rho_{liq.H_2}$ and $\rho_{ads.H_2}$ of GNPs. Here, microscopic structures of adsorbed H_2 molecules are pictured by taking account of adsorption types I and II to discuss the adsorbent and temperature dependence of superdense H_2 state observed above results. Type I adsorption isotherms for MSC-30 and MOF-177 are given by micropores filling of H_2 at low pressure due to the enhanced interaction with surface of adsorbent in narrow micropores. It can be considered that the adsorption with enhanced interaction makes the adsorption state to be the superdense H_2 state. In the case of Type II adsorption isotherms for GNPs, it is understood that the end point of steep H_2 uptake at low pressure corresponds to the completion of monolayer coverage and after that, H_2 uptake gradually increases by multilayer adsorption. In the BET theory, it is assumed that the multilayer adsorption region is equivalent to liquid state and the monolayer adsorption region just on the surface is more stable than the liquid state[32]. H.K. Livingston reported the anomalously low cross-sectional areas of H_2 at 20 K just on the Ni foil compared with

liquid density, indicating the anomalous highly condensed state just on the material surface similar to our result[33]. Therefore, we focused on the region of monolayer adsorption and evaluated the density of the monolayer adsorption ($\rho_{ads.H_2}^{mono}$) just on the material surface, because the density of multilayer adsorption ($\rho_{ads.H_2}^{multi}$) can be considered $\rho_{liq.H_2}$ at each phase transition point (see the "Evaluation of monolayer H_2 density" in the supplementary information). Based on the BET theory, it is possible to determine the ratio of the monolayer adsorption (R_{mono}) in the total adsorption for the analysis of $\rho_{ads.H_2}^{mono}$, and R_{mono} is evaluated to be 90% for MOF-177, 74% for MSC-30, and 42% for GNPs at 20.4 K and it shows a similar trend at other temperatures (Supplementary Table 1). As shown in the inset of Fig.3, $\rho_{ads.H_2}^{mono}$ of all the adsorbents reveal the constant value of 50 mmol/cm^3 without temperature dependence in the temperature range from 20.4 to 30.6 K (see also Supplementary Table. 1). Therefore, it was found that the superdense H_2 state is strongly related to the monolayer adsorption with direct interaction from material surface, irrespective of the adsorption types and temperature below critical point.

Focusing on the i-H_2 amount into the cell at 20.4 K below and above 0.1 MPa shown in Fig.1a, opposite tendency between MSC-30 and MOF-177 is recognized. In order to clarify this mystery, we evaluated the volumetric H_2 uptake ($\rho_{H_2}^{vol}$). Since $\rho_{H_2}^{multi}$ is regarded as $\rho_{liq.H_2}$ at each condition as discussed above, $\rho_{H_2}^{vol}$ is defined by

$$\rho_{H_2}^{vol} = \frac{M_{ads.H_2}^{mono}}{V_{ads.H_2}^{mono} + V_a}, \quad (1)$$

where $M_{ads.H_2}^{mono}$ is the H_2 amount of monolayer adsorption, $V_{ads.H_2}^{mono}$ and V_a are the volume of monolayer H_2 and adsorbents, respectively. $\rho_{H_2}^{vol}$ of each adsorbent are evaluated and shows constant value for each adsorbent with temperature, which are evaluated to be approximately 33 mmol/cm^3 for MOF-177, 34 mmol/cm^3 for MSC-30, and 17 mmol/cm^3 for GNPs (see the "Evaluation of volumetric H_2 uptake" in the supplementary information, Supplementary Fig. 2 and Supplementary Table 1). MSC-30 shows the highest value of $\rho_{H_2}^{vol}$, and it is comparable to $\rho_{liq.H_2}$ at 20.4 K and is 30% higher than $\rho_{liq.H_2}$ at 30.6 K. In order to know factors determining the value of $\rho_{H_2}^{vol}$, which is expressed by (see also the "discussion of volumetric H_2 adsorption" in the supplementary information)

$$\rho_{H_2}^{vol} = \frac{1}{1/\rho_{\mathrm{ads.H_2}}^{\mathrm{mono}} + 1/(\alpha\, S_a d_a)}, \tag{2}$$

where the parameter α is a constant value related to the adsorbed H_2 amount per surface area (mol/m^2) of adsorbent, S_a is the gravimetric surface area (m^2/g) of adsorbent, d_a is the real density (g/cm^3) of sample, that is to say, the value of $S_a d_a$ corresponds to the volumetric surface area (m^2/cm^3) of adsorbents. Since it was found that $\rho_{\mathrm{ads.H_2}}^{\mathrm{mono}}$ is a constant value based on the above discussion, equation (2) suggests that the volumetric surface area ($S_a d_a$) is a unique factor to determine the value of $\rho_{H_2}^{vol}$ under the superdense H_2 phenomena, resulting that MSC-30 having the highest volumetric surface area ($S_a d_a = 7436\ \mathrm{m^2/cm^3}$) shows the highest $\rho_{H_2}^{vol}$.

Conclusion

In this work, the cryogenic H_2 adsorption properties were investigated below critical point of H_2 (T_c = 33 K) on various kind of adsorbents by comparing the introduced H_2 amount into the cryogenic cell with and without adsorbents. We found the superdense H_2 adsorption having much higher density than that of liquid H_2, which is contrary to the general understanding that the density of adsorbed H_2 is believed to that of liquid H_2[6,9,11,24] as the upper limit. Based on the analysis focusing on the monolayer adsorption region, it is revealed that the density of adsorbed H_2 on adsorbents as monolayer state has the constant value of 50 mmol/cm^3 without temperature dependence in the temperature range from 20.4 to 30.6 K irrespective of the material type, which exceeds the density of solid H_2 (43 mmol/cm^3).

The gravimetric H_2 uptake (wt.%) under cryogenic temperature depends on the gravimetric surface area (m^2/g) as well as the trend of previous studies, which are 14.8 wt.% for MOF-177 (3950 m^2/g), 13.2 wt.% for MSC-30 (2860 m^2/g), 6.6 wt.% for GNPs (810 m^2/g) at 20.4 K, 0.1MPa. On the contrary to the trend of gravimetric H_2 uptake, MSC-30 shows the highest i-H_2 amount into the cryogenic cell with adsorbents, in other words the highest volumetric H_2 uptake (mmol/cm^3). We found that the volumetric surface area ($S_a d_a$) is a unique factor to determine the volumetric H_2 uptake under the superdense H_2 phenomena, resulting MSC-30 shows the highest constant value of 34 mmol/cm^3, followed in order by MOF-177 (33 mmol/cm^3), GNPs (17 mmol/cm^3) below 20.4-30.6 K. This low

temperature dependent properties of superdense H_2 state will show a great impact as a new method to suppress the H_2 loss caused by the temperature increase in the liquid H_2 storage tanks (boil-off). Further development of the optimum material and understanding of the phenomena of the superdense adsorbed state will show the more usefulness of the adsorbent on the cryogenic hydrogen storage techniques.

Methods

Textural properties of adsorbents.

Various adsorbents used in this work were obtained from different suppliers, which are metal organic frame works (MOF-177; Sigma-Aldrich), superactivated carbon (MSC-30; Kansai Coke and Chemicals Co., Ltd) and graphene nanoplatelets (GNPs; STREM chemicals). Prior to the measurement, all adsorbents were degassed at 200 ºC for 12 h under vacuum condition. Textural properties were determined by N_2 adsorption-desorption isotherms at 77 K using Sieverts' apparatus (Belsorp-max 12N-VP-LTC, Microtrac BEL). The gravimetric surface area (m^2/g) was evaluated by applying the Brunauer-Emmett-Teller (BET) theory to the N_2 adsorption isotherms in the relative pressure P/P_0 range of 0.03-0.06 for MOF-177, 0.03-0.06 for MSC-30, and 0.03-0.35 for GNPs. In general, the pressure region is applied up to $P/P_0 = 0.35$, for Type II adsorption like GNPs, however it is not suitable for Type I adsorption like MOF-177 and MSC-30 because the monolayer adsorption is completed at lower pressure than $P/P_0 = 0.35$. Here, we determined the appropriate pressure range by applying a method proposed by Rouquerol et al[34]. The total pore volume was determined from the nitrogen uptake at the relative pressure of $P/P_0 \approx 0.99$. The real density for each adsorbent was evaluated volumetrically with helium gas at 40 ºC using Sieverts' apparatus (Belsorp-max 12N-VP-LTC, Microtrac BEL). The volumetric surface area of MSC-30, MOF-177 and GNPs were calculated to be 6320, 6990 and 1780 m^2/g, respectively, by multiplying the gravimetric surface area by the real density.

Isothermal properties of cryogenic H_2 adsorption.

Cryogenic H_2 adsorption properties were investigated by a Sieverts' type apparatus provided by Suzuki Shokan Co., Ltd., and the sample cell (12.3 cm^3) was cooled by a He cryocooler (C200G) provided by Suzuki Shokan Co., Ltd., (see the diagram in Supplementary Fig.3). The system accurately measures the introduced H_2 (i-H_2) amount into the sample cell as following steps: 1. H_2 gas was introduced into a reservoir of known value at desired pressure; 2. the valve connected to sample cell was opened and the H_2 was introduced into the sample cell and wait for 5-10 min until temperature and pressure are stable; 3. The i-H_2 amount in the line part and the sample cell was calculated by the difference of H_2 amount in the reservoir between step 1 and 2, where the density of H_2 used in the calculation was obtained NIST website[26]; 4. The 1-3 steps were repeated until pressure in the sample cell is reached to 1.5 MPa. 5. The i-H_2 amount into the line part was evaluated by the measurement of step1-4 with blind gasket between the line part and the sample cell, and then that was subtracted from the i-H_2 amount into the line part and the sample cell. Prior to the measurement, all adsorbents were degassed at 200 ºC for 12 h under vacuum condition in a stainless tube, and 2.22 g of MOF-177, 1.50 of MSC-30 and 2.00 of GNPs were put into the sample cell in a glove box filled by highly purified Ar gas (>99.9999%). When the sample cell was connected to the cold head, Apiezon N high vacuum grease (Apiezon products M&L Materials LTD) was used to make close contact between the sample

cell and the cold head to obtain good thermal conductivity and less temperature gradient. Ar gas in the sample cell was evacuated to 1×10^{-4} MPa by rotary pump at room temperature, and the air in the vacuum insulation container was evacuated to 1×10^{-2} Pa by turbo molecular pump with diaphragm pump. Then, the sample cell was cooled by the He cryocooler and the temperature was adjusted to desired temperature by heater block with a temperature controller surrounding the sample cell. We carried out this measurement with and without adsorbents at 20.4, 23.3, 26.5, 30.6 K, which are below critical temperature (T_p=33 K). These temperatures were determined by the corresponding to the liquefaction pressure in the isotherms referred from NIST website[26]. The gravimetric H_2 uptake was evaluated by dividing the amount of adsorbed H_2 by the sample amount, where the contribution of gaseous hydrogen in the dead volume was withdrawn by the specific procedure (see also Supplementary Information).

Data availability

The data that support the findings of this study are available from the corresponding author upon reasonable request.

Reference

1. Schlapbach, L. & Züttel, A. Hydrogen storage materials for Mobile Applications. *Nature* **414**, 353–358 (2001).
2. Hirscher, M. *et al.* Materials for hydrogen-based energy storage – past, recent progress and future outlook. *J. Alloys Compd.* **827**, (2020).
3. Rzepka, M., Lamp, P. & De La Casa-Lillo, M. A. Physisorption of hydrogen on microporous carbon and carbon nanotubes. *J. Phys. Chem. B* **102**, 10894–10898 (1998).
4. Man Mohan, Vinod Kumar Sharma, Gayathri, E. Anil Kumar, V. G. Hydrogen storage in carbon materials. *Energy Storage* **1**, 1–26 (2019).
5. Sebastian Zuluaga, Pieremanuele Canepa, Kui Tan, Yves J Chabal, T. T. Study of van der Waals bonding and interactions in metal organic framework materials. *J. Phys. Condens. Matter* **26**, 15 (2014).
6. Züttel, A., Sudan, P., Mauron, P. & Wenger, P. Model for the hydrogen adsorption on carbon nanostructures. *Appl. Phys. A Mater. Sci. Process.* **78**, 941–946 (2004).
7. Zhao, X. B., Xiao, B., Fletcher, A. J. & Thomas, K. M. Hydrogen adsorption on functionalized nanoporous activated carbons. *J. Phys. Chem. B* **109**, 8880–8888 (2005).
8. Panella, B., Hirscher, M. & Roth, S. Hydrogen adsorption in different carbon nanostructures. *Carbon N. Y.* **43**, 2209–2214 (2005).
9. Kojima, Y. *et al.* Hydrogen adsorption and desorption by carbon materials. *J. Alloys Compd.* **421**, 204–208 (2006).
10. Yushin, G., Dash, R., Jagiello, J., Fischer, J. E. & Gogotsi, Y. Carbide-derived carbons: Effect of pore size on hydrogen uptake and heat of adsorption. *Adv. Funct. Mater.* **16**, 2288–2293 (2006).
11. Thomas, K. M. Hydrogen adsorption and storage on porous materials. *Catal. Today* **120**, 389–398 (2007).
12. Yürüm, Y., Taralp, A. & Veziroglu, T. N. Storage of hydrogen in nanostructured carbon materials. *Int. J. Hydrog. Energy* **34**, 3784–3798 (2009).
13. Nijkamp, M. G., Raaymakers, J. E. M. J., Van Dillen, A. J. & De Jong, K. P. Hydrogen storage using physisorption-materials demands. *Appl. Phys. A Mater. Sci. Process.* **72**, 619–623 (2001).
14. Langmi, H. W. *et al.* Hydrogen adsorption in zeolites A, X, Y and RHO. *J. Alloys Compd.* **356**–**357**, 710–715 (2003).
15. Li, Y. & Yang, R. T. Hydrogen storage in low silica type X zeolites. *J. Phys. Chem. B* **110**, 17175–17181 (2006).
16. Dong, J., Wang, X., Xu, H., Zhao, Q. & Li, J. Hydrogen storage in several microporous zeolites. *Int. J. Hydrog. Energy* **32**, 4998–5004 (2007).

17. Prasanth, K. P., Raj, M. C., Bajaj, H. C., Kim, T. H. & Jasra, R. V. Hydrogen sorption in transition metal modified mesoporous materials. *Int. J. Hydrog. Energy* **35**, 2351–2360 (2010).
18. Rosi, N. L. *et al.* Hydrogen storage in microporous metal-organic frameworks. *Science.* **300**, 1127–1129 (2003).
19. Hirscher, M. & Panella, B. Hydrogen storage in metal-organic frameworks. *Scr. Mater.* **56**, 809–812 (2007).
20. Murray, L. J., Dinc, M. & Long, J. R. Hydrogen storage in metal-organic frameworks. *Chem. Soc. Rev.* **38**, 1294–1314 (2009).
21. Suh, M. P., Park, H. J., Prasad, T. K. & Lim, D. W. Hydrogen storage in metal-organic frameworks. *Chem. Rev.* **112**, 782–835 (2012).
22. Ahmed, A. *et al.* Balancing gravimetric and volumetric hydrogen density in MOFs. *Energy Environ. Sci.* **10**, 2459–2471 (2017).
23. Chen, Z. *et al.* Balancing volumetric and gravimetric uptake in highly porous materials for clean energy. *Science.* **368**, 297–303 (2020).
24. Oh, H., Lupu, D., Blanita, G. & Hirscher, M. Experimental assessment of physical upper limit for hydrogen storage capacity at 20 K in densified MIL-101 monoliths. *RSC Adv.* **4**, 2648–2651 (2014).
25. Thommes, M. *et al.* Physisorption of gases, with special reference to the evaluation of surface area and pore size distribution (IUPAC Technical Report). *Pure Appl. Chem.* **87**, 1051–1069 (2015).
26. NIST Standard Reference Database Number 69. http://www.nist.gov/. https://webbook.nist.gov/chemistry/fluid/.
27. Saha, D., Wei, Z. & Deng, S. Equilibrium, kinetics and enthalpy of hydrogen adsorption in MOF-177. *Int. J. Hydrog. Energy* **33**, 7479–7488 (2008).
28. Keesom, W. H., de Smedt, J. & Mooy, H. H. On the crystal structure of para-hydrogen at liquid helium temperatures. *Proc R. Acad Amsterdam* **33**, 814 (1930).
29. Kogan, V. S., Lazarev, B. G. & Bulatova, R. F. The crystalline structure of hydrogen and deuterium. *Sov. Phys. JETP* **4**, (1957).
30. Silvera, I. F. The solid molecular hydrogens in the condensed phase: Fundamentals and static properties. *Rev. Mod. Phys.* **52**, 393–452 (1980).
31. Lin, C. Y., Gilbert, A. T. B. & Walker, M. A. Interstellar solid hydrogen. *Astrophys. J.* **736**, 16 (2011).
32. Brunauer, S., Emmett, P. H. & Teller, E. Adsorption of Gases in Multimolecular Layers. *J. Am. Chem. Soc.* **60**, 309–319 (1938).
33. Livingston, H. K. The cross-sectional areas of molecules adsorbed on solid surfaces. *J. Colloid Sci.* **4**, 447–458 (1949).

34. Rouquerol, J., Llewellyn, P. & Rouquerol, F. Is the BET equation applicable to microporous adsorbents. *Stud. Surf. Sci. Catal.* **160**, 49–56 (2007).

Acknowledgements

The authors are grateful to Prof. Hitoshi Saima and Dr. Keita Shinzato in Materials Engineering for Energy Conversion and Storage Labo., Hiroshima University for useful discussions in progressing this research.

Author contributions

K. S., N. O., H. M., T. O., M. S., L. P., and T. I. conceived the project and oversaw all the research phases. H. G., Y. K., and Y. I. carried out the experiments and data analysis. All the authors contributed to and commented on this paper.

Competing interests

The authors declare no competing interests.

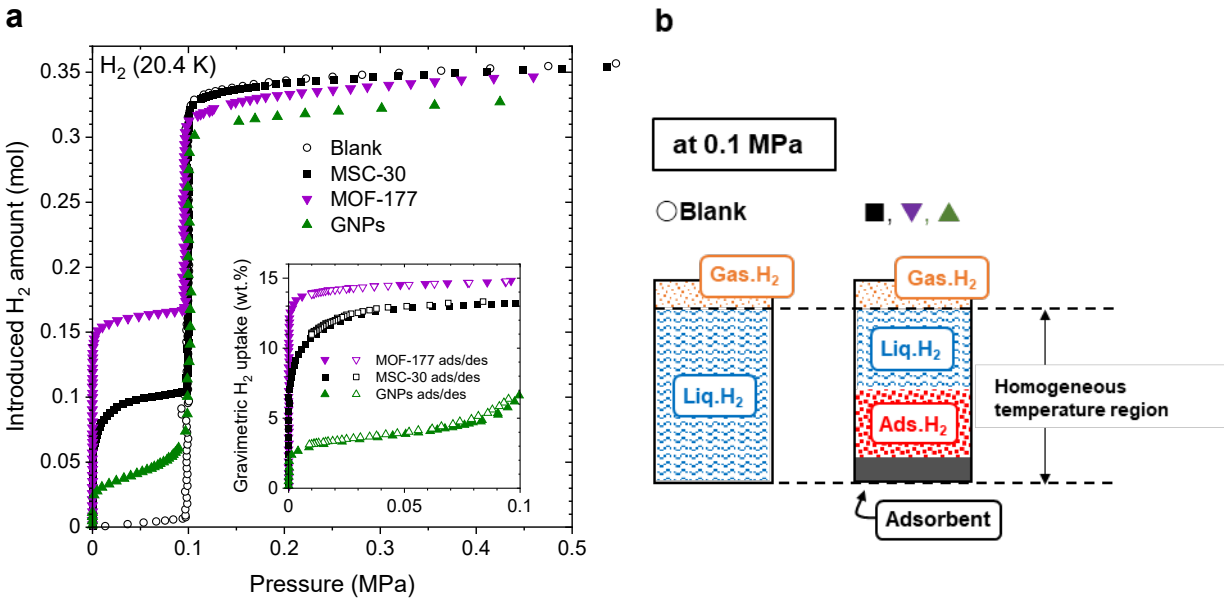

Fig. 1 Isothermal properties of H_2 introduction in the cell with and without adsorbents at 20.4 K. **(a)** Introduced H_2 amount in the empty cell (Blank) and in the cell with 2.22 g of MOF-177, 1.50 g of MSC-30 and 2.00 g of GNPs at 20.4 K. Inset is the gravimetric H_2 uptake of H_2 adsorption/desorption on each adsorbent, **(b)** Image of inside of cryogenic cell with and without adsorbent at 0.1 MPa.

Table 1 Textural properties of adsorbents (MOF-177, MSC-30, GNPs) and gravimetric H_2 uptake and density of adsorbed H_2 for each adsorbent at 20.4 K, 0.1 MPa.

		Adsorbent		
		MOF-177	**MSC-30**	**GNPs**
Gravimetric surface area	m^2/g	3950	2860	810
Total pore volume	cm^3/g	1.64	1.44	1.27
Apparent density	g/cm^3	1.6	2.6	2.2
Volumetric surface area	m^2/cm^3	6320	7436	1782
Gravimetric H_2 uptake (20.4 K)	wt.%	14.8	13.2	6.6
Density of adsorbed H_2 (20.4 K)	$mmol/cm^3$	**47.3 (134%)***	**43.1 (123%)***	**40.0 (114%)***

*The values in the brackets show the ratio compared to the density of liquid H_2 ($\rho_{liq.H_2} = 35.2\ \mathrm{mmol/cm^3}$, at 20.4 K, 0.1 MPa)

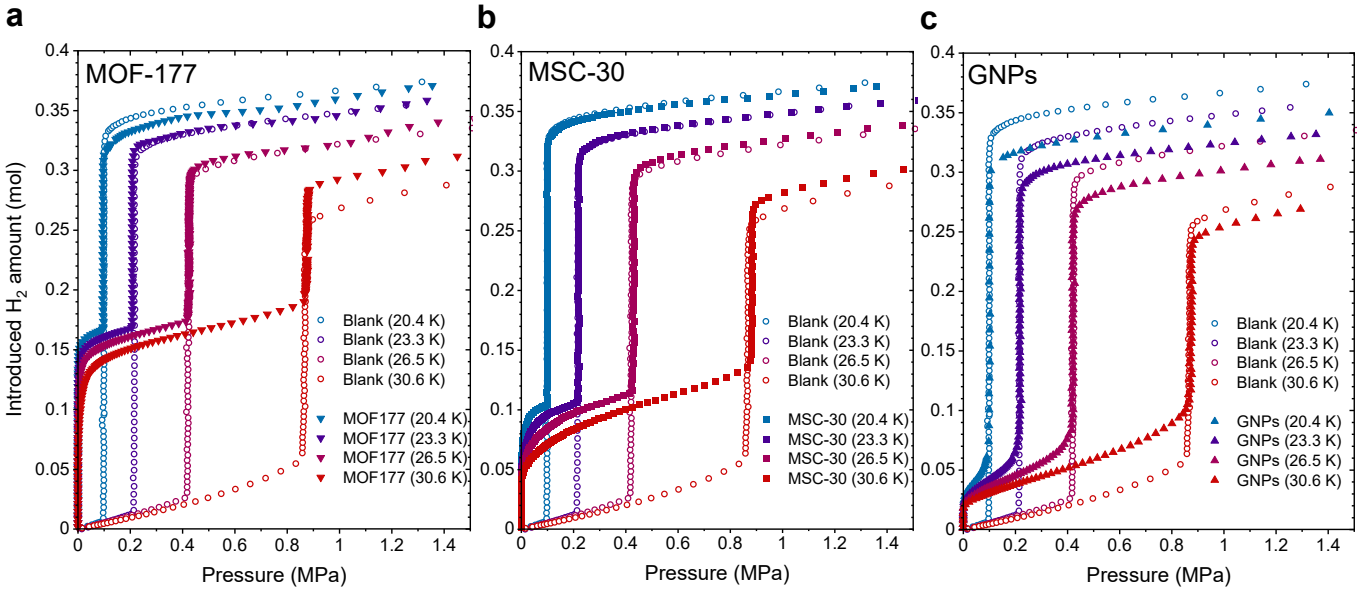

Fig.2 Temperature dependence of isothermal properties for H_2 introduction into the empty cell (Blank) and into the cell with **(a)** 2.22 g of MOF-177, **(b)** 1.50 g of MSC-30 and **(c)** 2.00 g of GNPs at 20.4, 23.3, 26.5, 30.6 K, respectively.

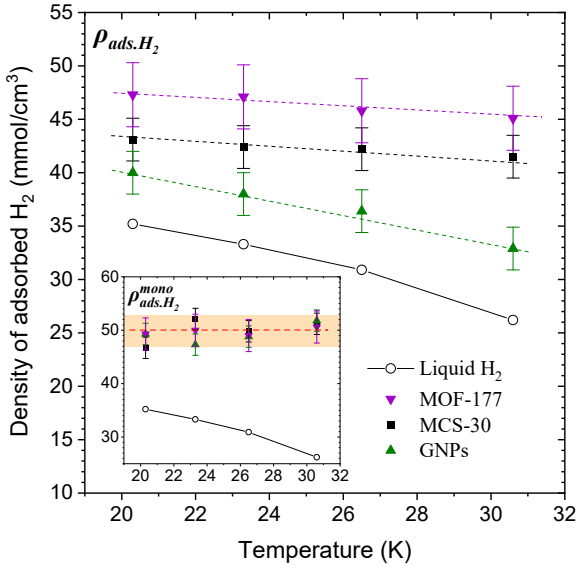

Fig. 3 Temperature dependence of the density of adsorbed H_2 compared to that of liquid H_2. The density of adsorbed H_2; $\rho_{ads.H_2}$ and monolayer H_2; $\rho^{mono}_{ads.H_2}$ (inset figure) at 20.4, 23.3, 26.5, 30.6 K on MOF-177. MSC-30 and GNPs.

Supplementary Files

This is a list of supplementary files associated with this preprint. Click to download.

- supplementaryinformation.docx